Scale of plume clustering in large-Prandtl-number convection

Scale of plume clustering in large-Prandtl-number convection

Sara Lenzi
Graduate School in Physics and Astrophysics, University of Torino, Turin 10125, Italy
and Institute of Geosciences and Earth Resources (IGG), National Research Council (CNR), Pisa 56124, Italy

Jost von Hardenberg
Department of Environment, Land, and Infrastructure Engineering, Politecnico di Torino, Turin 10129, Italy

Antonello Provenzale*
Institute of Geosciences and Earth Resources (IGG), National Research Council (CNR), Pisa 56124, Italy

(Received 21 May 2020; accepted 10 April 2021; published 14 May 2021)

Clustering of plumes in turbulent Rayleigh-Bénard convection has been numerically observed in low-Prandtl-number fluids. In this framework, turbulent plumes undergo a phase-separation process leading to large-scale clusters and circulations, sometimes called plume superstructures and reminiscent of solar granulation and supergranulation. On the other hand, the possible presence of large-scale plume aggregates has not been explored in the case of large values of the Prandtl number, Pr, relevant to geological settings such as convection in planetary interiors. Here we address this problem and numerically explore the behavior of plume ensembles in turbulent convection at very high Prandtl number values, including the case $\mathrm{Pr} \to \infty$. The results indicate the presence of plume clustering, albeit at smaller scale, also for large Pr number fluids, suggesting interesting consequences for mantle convection processes.

DOI: 10.1103/PhysRevE.103.053103

I. INTRODUCTION

Natural convection in fluids develops whenever an unstable density stratification is perturbed [1–3]. Two central parameters of fluid convection are the Rayleigh number, Ra, measuring the strength of buoyancy forces with respect to viscosity and thermal diffusion, and the Prandtl number, Pr, measuring the ratio of kinematic viscosity to thermal diffusivity. In turbulent convection, at values of $\mathrm{Ra} \gg 1$, the dynamics is characterized by the presence of intense plumes carrying heat upwards. In the simple case of fluid convection bounded above and below by two rigid horizontal plates kept at different temperature (with the lower plate at higher temperature than the upper), hot rising plumes detach from the boundary layer close to the lower plate and cold plumes descend from the upper boundary layer. In both cases, heat is transported upwards.

In past years, it was shown that at small and moderate values of the Prandtl number, turbulent plumes undergo a phase-separation process leading to distinct clusters of hot and cold plumes [4–8]. Associated with plume clustering is the birth of plume networks and fluid circulations at scales much larger than the horizontal size of the plumes [9]. Such behavior is, at least conceptually, reminiscent of the granulation and supergranulation observed in solar convection [10,11].

On the other hand, different natural convective settings, such as convection in a planetary mantle, are characterized by very large values of the Prandtl number, $\mathrm{Pr} \to \infty$. In such cases, it is not clear whether a plume clustering process, associated with large-scale circulations, is still present. To explore this problem, here we focus on a simplified, conceptual setting and numerically study the effects generated by a very large Prandtl number on the convection dynamics of a Newtonian Navier-Stokes fluid in the Boussinesq approximation. In this way, we eliminate other effects associated, for example, to phase transitions, complex rheology, and non-Newtonian behavior, and focus purely on the Prandtl number dependence of large-scale convective structures. The results of the analysis for values of Ra between 10^5 and 10^8, as detailed below, indicate that plume clustering and the associated large-scale circulations persist also at large values of the Prandtl number. The scale of the plume clusters, however, decreases with increasing Prandtl number and it stabilizes at a value close to the layer depth for $\mathrm{Pr} \to \infty$.

II. MODEL AND METHODS

The model equations adopted here describe incompressible fluid dynamics in the Boussinesq approximation [3,12]. We assume a fluid layer bounded above and below by two rigid horizontal plates kept at constant temperature, with the lower plate warmer than the upper. The dynamics is described by the equations for momentum, energy, and mass conservation that, in nondimensional form, are written as:

$$\frac{\partial \mathbf{u}}{\partial t} + (\mathbf{u}\cdot\nabla)\mathbf{u} = -\nabla p + \mathrm{PrRa}T\hat{\mathbf{z}} + \mathrm{Pr}\nabla^2\mathbf{u}, \tag{1}$$

$$\frac{\partial T}{\partial t} + (\mathbf{u}\cdot\nabla)T = \nabla^2 T, \tag{2}$$

$$\nabla\cdot\mathbf{u} = 0, \tag{3}$$

*Corresponding autor: antonello.provenzale@cnr.it

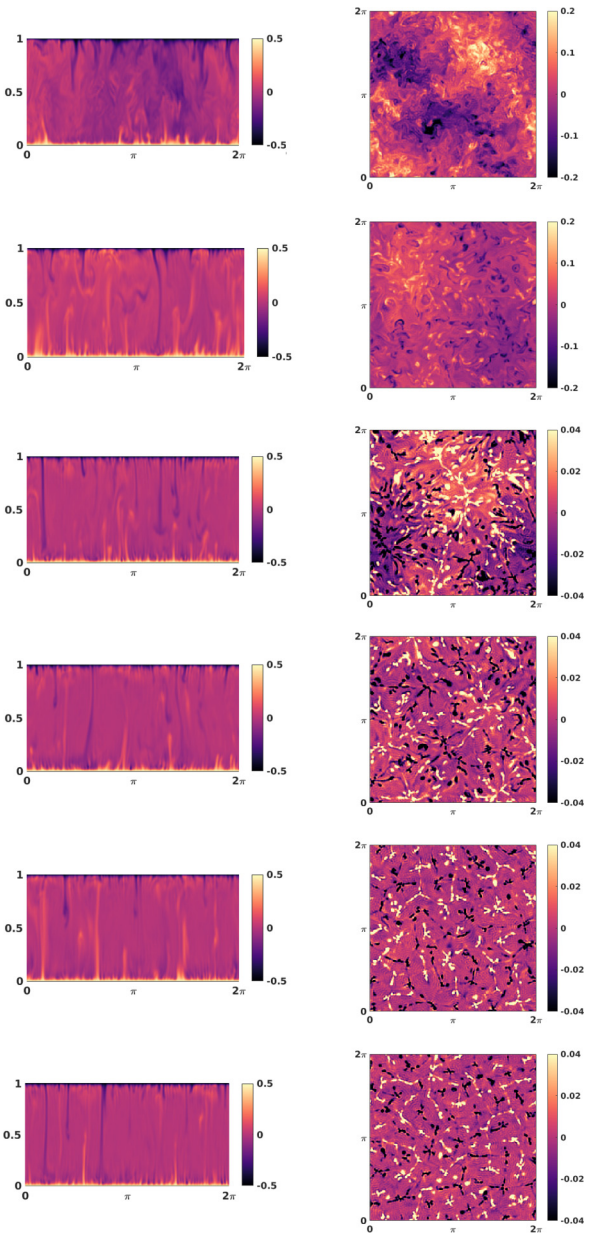

FIG. 1. Vertical (left) and horizontal (right) sections of the temperature field in the statistically stationary regime at $t = 0.06\tau_\kappa$. From top to bottom: Pr = 1, 10, 10^2, 3×10^2, 10^3 and Pr $\to \infty$. All cases are for Ra = 10^7. Horizontal sections are taken at the midplane $z = 0.5$ and vertical sections are taken at $y = \pi$.

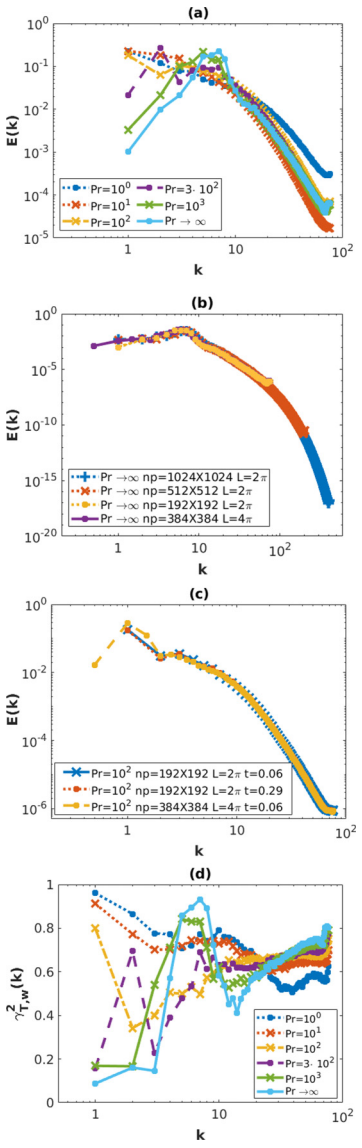

FIG. 2. (a) Energy spectra as a function of the horizontal radial wave number k, averaged along z and in the time interval $t \in [0.05 - 0.06]\tau_\kappa$, for different values of Pr. A peak at the largest scale is visible up to Pr = 10^2; for larger values of Pr the peak moves to higher values of k and it reaches a scale comparable to the depth of the domain for Pr $\to \infty$. (b) Energy spectra for Pr $\to \infty$, with different spatial resolutions and aspect ratio. The spectra show that increasing the resolution does not modify the shape of the spectrum, simply adding low-energy modes at high wave number. Analogously, doubling the aspect ratio does not modify the rest of the spectrum, simply adding a lower-energy mode at the lowest wave number (purple, solid line). (c) Energy spectra for Pr = 10^2 for aspect ratio $L = 2\pi$ respectively in the time intervals [0.05–0.06]τ_κ (blue, solid crossed) and [0.29–0.30]τ_κ (orange, dotted), and for aspect ratio $L = 4\pi$ in the interval [0.05–0.06]τ_κ (yellow, dashed). The spectra show that the system has reached a statistically stationary state and confirm that increasing the aspect ratio does not change the behavior. (d) Coherence spectra as a function of the horizontal radial wave number for different values of Pr, with Ra = 10^7 and $L = 2\pi$. Coherence spectra are averaged in the interval $t \in [0.05 - 0.06]\tau_\kappa$ and along z. The peak progressively moves to smaller spatial scales for Pr $\geqslant 3 \times 10^2$.

where $\mathbf{x} = (x, y, z)$, with z pointing upwards, $\mathbf{u} = (u, v, w)$ is the three-dimensional velocity, and $T(\mathbf{x}, t)$ is the temperature field. The above equations were nondimensionalized using the scales provided by the fluid layer thickness, D, the diffusive time, $\tau_\kappa = D^2/\kappa$ where κ is the thermal diffusivity, and the imposed temperature difference between the plates, ΔT. The velocity is scaled by κ/D. The Prandtl number is Pr = ν/κ where ν is the kinematic viscosity and the Rayleigh number is Ra = $\frac{g\beta\Delta T D^3}{\nu\kappa}$ where g is the acceleration of gravity

and β is the coefficient of thermal expansion of the fluid. In this work, fixed temperature and no slip velocity boundary conditions are adopted at the top and bottom, while periodic boundary conditions are assumed in the horizontal directions.

In the limit for $\mathrm{Pr} \to \infty$, assuming a finite value of Ra, the equations become the following:

$$\nabla p - \mathrm{Ra} T \hat{\mathbf{z}} - \nabla^2 \mathbf{u} = 0, \tag{4}$$

$$\frac{\partial T}{\partial t} + (\mathbf{u} \cdot \nabla) T = \nabla^2 T, \tag{5}$$

$$\nabla \cdot \mathbf{u} = 0. \tag{6}$$

In this configuration, the velocity field is determined by the temperature and pressure fields, since acceleration is neglected together with the nonlinear inertial term. A nonlinear advection term is still present in the heat equation. In the following, we consider values of the Rayleigh number between $\mathrm{Ra} = 10^5$ and $\mathrm{Ra} = 10^8$ and explore values of the Prandtl number $\mathrm{Pr} \geqslant 1$, with special attention to the case $\mathrm{Pr} \to \infty$.

To numerically solve Eqs. (1)–(3) for a finite value of the Pr number, we use the code already employed in Refs. [5,9]. For the $\mathrm{Pr} \to \infty$ case, a nontrivial problem of setting additional boundary conditions arises [13]. The additional boundary conditions on pseudopressure were implemented following the influence matrix method [14]. The numerical code is pseudospectral in the horizontal (with 4/5 dealiasing) and adopts a nonuniform finite difference grid in the vertical. The code is open source and available on GitHub [15]. Most simulations are run on a squared-basin domain with aspect ratio $L = L_x/D = L_y/D = 2\pi$, using 129 grid points in the vertical and 192^2 points in the horizontal. Cases with a larger horizontal domain ($L = 4\pi$) or with higher resolution are considered to answer specific questions, as discussed below.

As in Ref. [5], the kinetic energy spectrum $E(k)$ is obtained as a function of the horizontal radial wave number $k = \sqrt{k_x^2 + k_y^2}$, integrating over the horizontal wave-number angle. Estimates of the plume cluster size are provided by the scale at which the kinetic energy spectrum is maximum, $\lambda_M = 2\pi/k_M$, and by the integral scale $\lambda_I(t) = \frac{\int (E(k,t)/k)dk}{\int E(k,t)dk}$, already defined in Parodi *et al.* [5].

Recently, in Ref. [7] it was shown that estimates of clustering based only on the analysis of the energy spectra can be insufficient, suggesting the additional use of the spectral coherence between the vertical velocity and temperature fields, $\gamma^2_{T,w}(k) = \frac{|\Phi_{T,w}(k)|^2}{\Phi_{T,T}(k)\Phi_{w,w}(k)}$, calculated from the one-side cospectrum $\Phi_{T,w}(k)$ where w is the vertical component of velocity. Plume clustering is then marked by a low-k peak in the coherence spectrum.

III. RESULTS

Figure 1 shows the vertical (left) and horizontal (right) sections of the temperature field at $t = 0.06\tau_\kappa$ for $\mathrm{Pr} = 1$, 10,

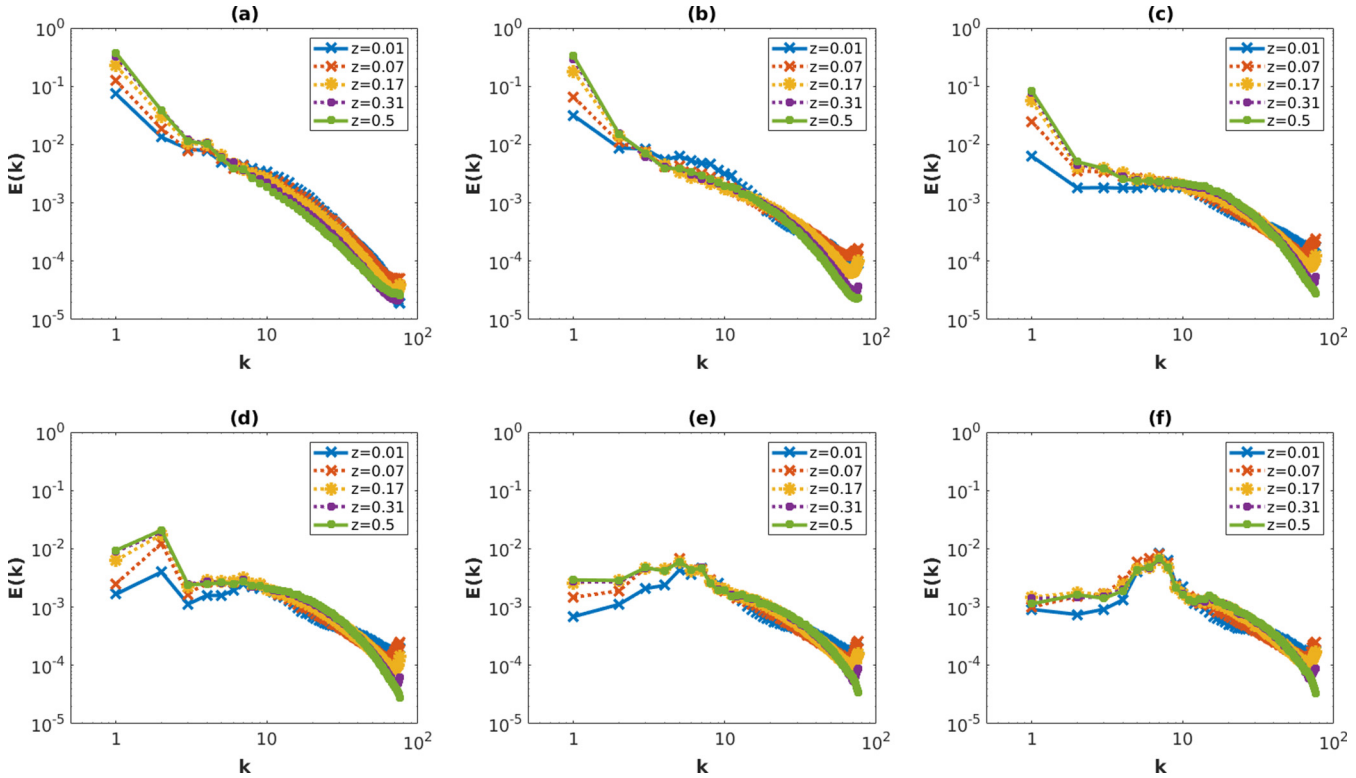

FIG. 3. Energy spectra as a function of the horizontal radial wave number and z for different values of Pr at $\mathrm{Ra} = 10^7$ and $L = 2\pi$. Panels (a) to (f) report results for $\mathrm{Pr} = 1$, 10, 10^2, 3×10^2, 10^3 and $\mathrm{Pr} \to \infty$ respectively. Spectra are averaged in the interval $t \in [0.05 - 0.06]\tau_\kappa$. While for small Pr a peak at the lower k is evident, for all z, the peak progressively moves to higher k (smaller spatial scales) for $\mathrm{Pr} \geqslant 3 \times 10^2$, indicating the presence of plume clusters with reduced size with respect to the lower-Pr cases.

10^2, 3×10^2, 10^3 and $\mathrm{Pr} \to \infty$, with $\mathrm{Ra} = 10^7$. Horizontal sections are taken at the midplane $z = 0.5$. As expected, the late-time dynamics for $\mathrm{Pr} = 1$ visually reveals the presence of large-scale plume clusters. On the other hand, similar clusters, albeit of smaller size, appear also at larger values of the Prandtl number.

To quantitatively identify possible plume clusters we turn to energy and coherence spectra [5,7]. Figure 2 shows the energy spectra for different values of Pr, averaged over time and along the vertical. In Fig. 2(a), the spectrum for $\mathrm{Pr} = 1$ at $t = 0.06\tau_\kappa$ shows a maximum at the lowest wave number, consistent with Ref. [5]. The same peak is observed for $\mathrm{Pr} = 10$ and $\mathrm{Pr} = 10^2$, while the cases $\mathrm{Pr} = 3 \times 10^2$, $\mathrm{Pr} = 10^3$, and $\mathrm{Pr} \to \infty$ show a pile-up of kinetic energy at a slightly larger wave number, indicating that the plume clusters have smaller size. Figure 2(d), at the bottom, shows that also the coherence spectrum is strongly peaked at $k = 1$ for $\mathrm{Pr} = 1$, $\mathrm{Pr} = 10$, and $\mathrm{Pr} = 100$, while the coherence peak moves to a slightly larger wave number for larger values of Pr.

The energy spectra for individual horizontal layers (i.e., as a function of z) are shown in Fig. 3 for different values of the Pr number and $\mathrm{Ra} = 10^7$. A peak at the lower k is evident for low Pr number while, for $\mathrm{Pr} \geqslant 3 \times 10^2$, the peak moves to higher k values at all z levels, confirming the presence of a plume cluster structure with smaller size, coherently throughout the domain.

The shapes of the spectra do not change by increasing spatial resolution at fixed aspect ratio, simply opening up new modes in the high-k domain, as illustrated in Fig. 3(b) of Fig. 2 for the case $\mathrm{Pr} \to \infty$. Higher resolutions, on the other hand, allow us to better depict the small-scale structure of the convective flows, as shown in the two upper panels of Fig. 4. In particular, the ascending and descending ridges that connect the plumes acquire a thinner and more continuous nature at high resolution.

We also run the simulations in larger domains with $L = 4\pi$, shown in Figs. 2(b) and 2(c) for $\mathrm{Pr} \to \infty$ and $\mathrm{Pr} = 10^2$, respectively, to verify whether the cluster scale could depend on the domain size. In all cases, the results do not change. For a larger domain, the effect is simply to add a lower energy mode in the spectrum at low k ($k = 0.5$). A visual illustration of this behavior is provided by the two temperature sections shown in Fig. 5. We also run the simulations for much longer times, up to $t = 0.3\tau_\kappa$ [shown in Fig. 2(c) for the case $\mathrm{Pr} = 10^2$], to verify whether a statistically stationary state has been

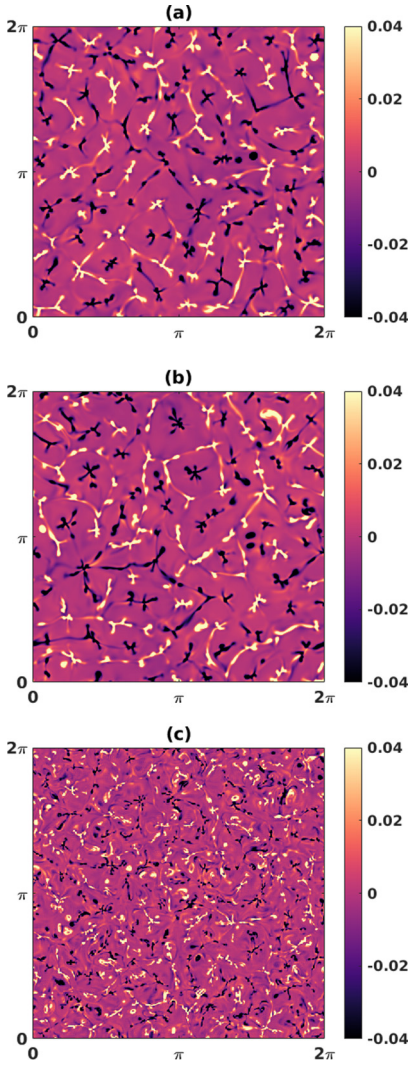

FIG. 4. [(a) and (b)] Midplane sections of the temperature field for $\mathrm{Pr} \to \infty$, $\mathrm{Ra} = 10^7$ at $t = 0.06\tau_\kappa$, with resolution respectively $512 \times 512 \times 193$ and $1024 \times 1024 \times 193$ grid points. (c) Midplane section of the temperature field for $\mathrm{Pr} \to \infty$, $\mathrm{Ra} = 10^8$ at $t = 0.06\tau_\kappa$, with resolution $512 \times 512 \times 193$ grid points.

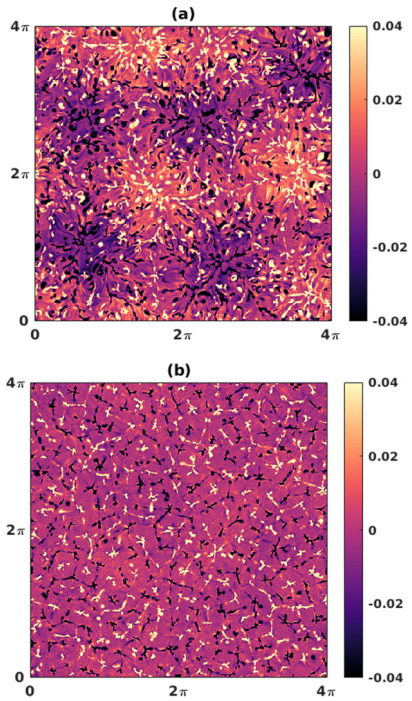

FIG. 5. Midplane sections of the temperature field for $\mathrm{Pr} = 100$ (a) and $\mathrm{Pr} \to \infty$ (b) for $\mathrm{Ra} = 10^7$ at $t = 0.06\tau_\kappa$, with resolution $384 \times 384 \times 129$ grid points and aspect ratio 4π. In the top panel, the size of the plume clusters is approximately 2π. In the bottom panel, the size of cluster is of the order of the domain depth. In both cases, the size of the plume aggregates is independent of the aspect ratio if the latter is larger than 2π.

reached. In all cases, no further changes in the spectra were observed.

The spatial scale at which the energy spectrum is maximum, λ_M, and the integral scale λ_I provide a quantitative measure of the size of the large-scale clusters [5,7]. Figure 6 shows the temporal evolution of these scales for different values of the Prandtl number. For $\mathrm{Pr} = 1$, λ_M reaches the domain scale and the integral scale λ_I grows with time, as observed in Ref. [5]. The same happens up to $\mathrm{Pr} = 10^2$, while a different behavior is present for $\mathrm{Pr} = 3 \times 10^2$, $\mathrm{Pr} = 10^3$, and $\mathrm{Pr} \to \infty$. In such cases, the maximum and integral spectral scales further confirm that at large values of the Prandtl number the plume aggregates have smaller size. The average horizontal size of the plumes, as obtained by a plume census algorithm such as that described in Ref. [5], does not grow with time and the number of plumes is statistically stationary, confirming that, also at large Pr, plume clustering is not associated with plume merging.

Figure 7(a) reports the values of λ_M (red, diamonds) and λ_I (blue, crosses) at $t = 0.06\tau_\kappa$ for the different values of the Prandtl number explored in this work and for $\mathrm{Ra} = 10^7$. For $\mathrm{Pr} > 100$, the clustering scales become smaller than 2π, converging to about one (the depth of the convecting layer) for $\mathrm{Pr} \to \infty$. For the case $\mathrm{Ra} = 10^7$, the reduction of the plume cluster scale takes place between $\mathrm{Pr} = 10^2$ and $\mathrm{Pr} = 3 \times 10^2$, while it happens at lower Pr values for $\mathrm{Ra} = 10^5$, as reported in Ref. [6].

The lower panel of Fig. 7 shows the cluster scales, for the case $\mathrm{Pr} \to \infty$, for different values of the Rayleigh number from $\mathrm{Ra} = 10^5$ to $\mathrm{Ra} = 10^8$. An example of the temperature field for $\mathrm{Ra} = 10^8$ is shown in the lower panel of Fig. 4. The results reveals only a weakly increasing trend of the cluster scale with the value of the Rayleigh number.

IV. DISCUSSION AND CONCLUSIONS

Plume clustering is an important process in turbulent Rayleigh-Bénard convection [4,5]. At the values of the Rayleigh number explored in past works, convective plumes undergo a phase-separation process, creating large ensembles of hot and cold plumes that generate large-scale structures and circulation cells at scales much larger than the plume size. Such circulation cells are reminiscent of the large-scale wind discussed in early studies of convection [16–18]. For $\mathrm{Ra} = 10^7$ and values of the Prandtl number around one (that is, when the diffusive and viscous times are approximately equal), the plume clusters have a wavelength of about 2π [9].

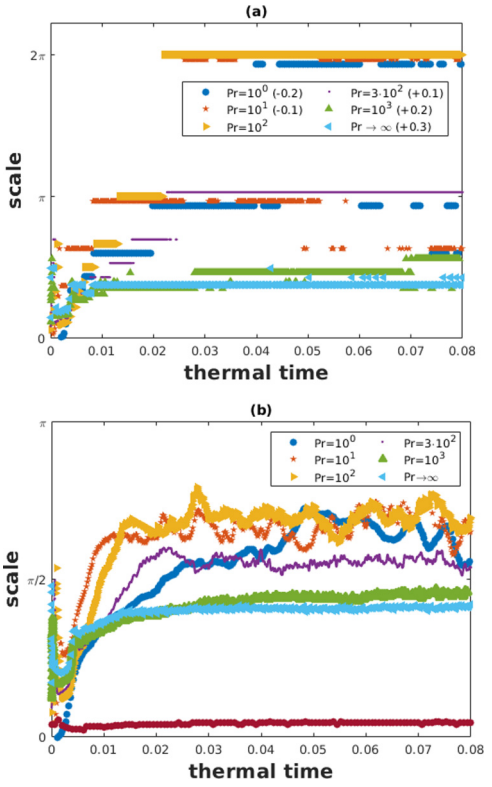

FIG. 6. Temporal evolution of the scale at which the energy spectrum is maximum, λ_M (a) and of the integral scale λ_I (b), for $\mathrm{Pr} = 1$, $\mathrm{Pr} = 10$, $\mathrm{Pr} = 10^2$, $\mathrm{Pr} = 3 \times 10^2$, $\mathrm{Pr} = 10^3$, and $\mathrm{Pr} \to \infty$. For all cases, $\mathrm{Ra} = 10^7$. Time is in unit of the diffusive time τ_κ. In the lower panel, also the average size of the individual plumes is plotted, showing that it does not change with time after the initial formation phase. In the upper panel, in order to avoid overlapping, data are shifted with respect to the $\mathrm{Pr} = 10^2$ case, as indicated in the legend.

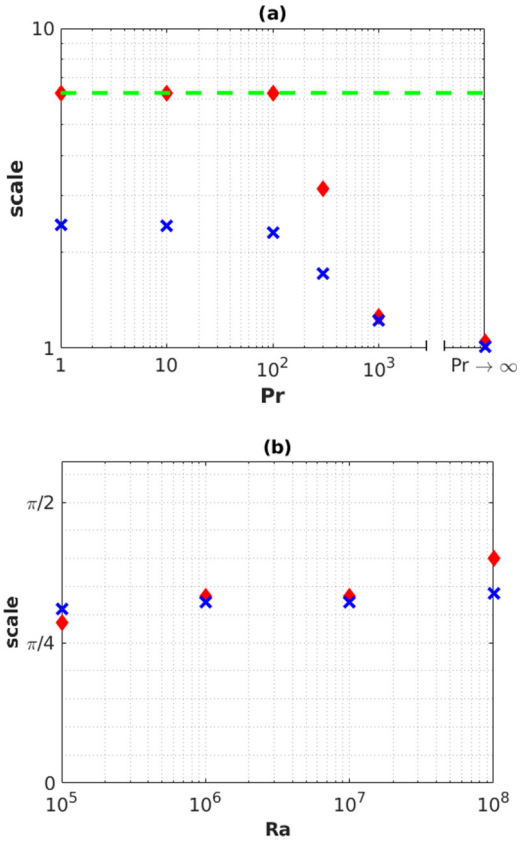

FIG. 7. (a) Maximum energy scale, λ_M (red, diamonds) and maximum value of the integral scale λ_I (blue, crosses) as a function of the Prandtl number for $\mathrm{Ra} = 10^7$. (b) Maximum energy scale, λ_M (red, diamonds) and maximum value of the integral scale λ_I (blue, crosses) as a function of the Rayleigh number for $\mathrm{Pr} \to \infty$. Each value is obtained from a mean over the interval $t \in [0.05 - 0.06]\tau_\kappa$.

More recently, the dependence of plume clustering on the value of the Prandtl number was explored [6], finding indications of a weakening of plume clustering at values of the Prandtl number larger than 1. Here, we addressed the high-Pr regime and numerically explored a range of values from $\mathrm{Pr} = 1$ to $\mathrm{Pr} \to \infty$ for $\mathrm{Ra} = 10^7$. The case for $\mathrm{Pr} \to \infty$ was explored also for values of the Rayleigh number in the range $[10^5 - 10^8]$. Our results indicate the persistence of the plume clustering process for any value of the Prandtl number, albeit with a cluster scale decreasing to about the depth of the convecting layer for $\mathrm{Pr} \to \infty$.

In the present approach, we took the limit for large Prandtl number while keeping the Rayleigh number constant, a choice that makes the flow less turbulent. Indeed, the simulations show a much smoother circulation at large Pr. Coherent small-scale plumes are always present, but they move around more slowly for increasing values of the Prandtl number. On the other hand, the kinetic energy continues to move to larger scales, so that both plume clusters and large-scale circulations are formed. This process is reminiscent of the weakly nonlinear conditions studied in Ref. [18], where large-scale winds were shown to form also in a low-mode truncation of the fluid dynamical equations.

In past works, different interpretations have been provided to explain the phenomenon of plume clustering [5,9], although a complete understanding of this phenomenon is still lacking. One interpretation refers to the ascending and descending plumes action against the boundaries. At low Pr numbers, the horizontal velocity divergence generated by the hot (cold) plumes splashing on the boundary is thought to push the roots of the cold (hot) plumes away, forcing them to become closer to each other and leading to the formation of aggregates, in a process reminiscent of phase separation. The efficiency of this process presumably depends also on the thickness of the viscous boundary layer. At higher values of the Prandtl number, such thickness becomes larger, potentially reducing the splashing effects of the impinging plumes and leading to a smaller scale of the plume aggregates. Further analysis is clearly needed to understand the process of plume clustering in general, besides its Pr-number dependence.

Our findings can bear interesting consequences on natural convective systems with large values of the Prandtl number. For example, provided these results may inform on the much more complex case of mantle convection, one could infer that plume clustering and large-scale circulations should be present in planetary interiors, possibly favoring organization of the convection on scales much larger than the size of the individual plumes.

ACKNOWLEDGMENTS

This work benefited of the CINECA ISCRA grants SIPRACo3 and SIPRACo4. Support was provided by the project ASI-INAF 2018-25-HH.0 "Scientific activities for JUICE phase C/D." Part of the computational resources were provided by HPC@POLITO [19].

[1] Lord Rayleigh, LIX, On convection currents in a horizontal layer of fluid, when the higher temperature is on the under side, Lond. Edinb. Dubl. Philos. Mag. J. Sci. **32**, 529 (1916).

[2] H. Bénard and D. Avsec, Travaux récents sur les tourbillons cellulaires et les tourbillons en bandes. Applications à l'astrophysique et à la météorologie, J. Phys. Rad. **9**, 486 (1938).

[3] S. Chandrasekhar, *Hydrodynamic and Hydromagnetic Stability*, The International Series of Monographs in Physics (Clarendon Press, Oxford University Press, 1961), p. 652.

[4] T. Hartlep, A. Tilgner, and F. H. Busse, Large Scale Structures in Rayleigh-Bénard Convection at High Rayleigh Numbers, Phys. Rev. Lett. **91**, 064501 (2003).

[5] A. Parodi, J. von Hardenberg, G. Passoni, A. Provenzale, and E. A. Spiegel, Clustering of Plumes in Turbulent Convection, Phys. Rev. Lett. **92**, 194503 (2004).

[6] A. Pandey, J. D. Scheel, and J. Schumacher, Turbulent superstructures in Rayleigh-Bénard convection, Nat. Commun. **9**, 2118 (2018).

[7] D. Krug, D. Lohse, and R. J. A. M. Stevens, Coherence of temperature and velocity superstructures in turbulent Rayleigh–Bénard flow, J. Fluid Mech. **887**, A2-1 (2020).

[8] R. J. A. M. Stevens, A. Blass, X. Zhu, R. Verzicco, and D. Lohse, Turbulent thermal superstructures in Rayleigh-Bénard convection, Phys. Rev. Fluids **3**, 041501(R) (2018).

[9] J. von Hardenberg, A. Parodi, G. Passoni, A. Provenzale, and E. Spiegel, Large-scale patterns in Rayleigh–Bénard convection, Phys. Lett. A **372**, 2223 (2008).

[10] E. A. Spiegel, The effect of radiative transfer on convective growth rates, Astrophys. J. **139**, 959 (1964).

[11] F. Rincon and M. Rieutord, The sun's supergranulation, Liv. Rev. Solar Phys. **15**, 6 (2018).

[12] F. Busse, High Prandtl number convection, Phys. Earth Planet. Inter. **19**, 149 (1979).

[13] D. Rempfer, On boundary conditions for incompressible Navier-Stokes problems, Appl. Mech. Rev. **59**, 107 (2006).

[14] L. Quartapelle, *Numerical Solution of the Incompressible Navier-Stokes Equations*, Vol. 113 (Birkhäuser, Basel, 2013).

[15] J. von Hardenberg, RBsolve: Pseudospectral Rayleigh-Bénard Solver, https://github.com/jhardenberg/rbsolve.

[16] E. A. Spiegel, Thermal turbulence at very small Prandtl number, J. Geophys. Res. (1896-1977) **67**, 3063 (1962).

[17] E. A. Spiegel, Convection in stars I. Basic Boussinesq convection, Annu. Rev. Astron. Astrophys. **9**, 323 (1971).

[18] L. N. Howard and R. Krishnamurti, Large-scale flow in turbulent convection: A mathematical model, J. Fluid Mech. **170**, 385 (1986).

[19] HPC@POLITO, a project of Academic Computing within the Department of Control and Computer Engineering at the Politecnico di Torino, http://www.hpc.polito.it.